Constraint-based fracture mechanics analysis of cylinders with internal circumferential cracks

Michael Bach and Xin Wang[*]

*Department of Mechanical and Aerospace Engineering, Carleton University,
Ottawa, Ontario K1S 5B6, Canada*

Abstract. In this paper, constraint-based fracture mechanics analyses of hollow cylinders with internal circumferential crack under tensile loading are conducted. Finite element analyses of the cracked cylinders are carried out to determine the fracture parameters including elastic T-stresses, and fully-plastic J-integrals. Linear elastic finite element analysis is conducted to obtain the T-stresses, and elastic-plastic analysis is conducted to obtain the fully plastic J-integrals. A wide range of cylinder geometries are studied, with cylinder radius ratios of $r_i/r_o = 0.2$ to 0.8 and crack depth ratio $a/t = 0.2$ to 0.8. Fully plastic J-integrals are obtained for Ramberg-Osgood power law hardening material of $n = 3$, 5 and 10. These fracture parameters are then used to construct conventional and constraint-based failure assessment diagrams (FADs) to determine the maximum load carrying capacity of cracked cylinders. It is demonstrated that these tensile loaded cylinders with circumferential cracks are under low constraint conditions, and the load carrying capacity are higher when the low constraint effects are properly accounted for, using constraint-based FADs, comparing to the predictions from the conventional FADs.

Keywords: circumferential crack; cylinder; J-integral; stress intensity factor; T-stress; failure assessment; constraint effect

1. Introduction

Conventional fracture mechanics is based on the concept that the stress fields at the vicinity of the crack can be characterized by a single fracture mechanics parameter, i.e., the stress intensity factor K or the J-integral. When the crack tip plastic-zone is small, the stress intensity factor is commonly used to characterize the stresses at the crack tip. If substantial plasticity is developed around the crack tip, the stress field inside the plastic zone is characterized by the J-integral. However, it has been well-established that conventional single-parameter fracture mechanics based on the K or J-integral could be overly conservative in failure assessments for the low constraint conditions (Ainsworth and O'Dowd 1995, Lidbury *et al*. 2006). The conventional failure assessment methods based on single-parameter fracture mechanics use a lower bound fracture toughness taken from highly constrained test specimens. This approach could translate to unnecessary economical loss in maintenance and replacement of these cracked structures before they need to be replaced.

∗Corresponding author, Professor, E-mail: xwang@mae.carleton.ca

Over the past two decades, a two-parameter, constraint-based fracture mechanics has been developed to account for this constraint effect to provide a more realistic fracture analysis for the low constrained crack geometries (Du and Hancock 1991, Betegon and Hancock 1991). Constraint-based fracture mechanics uses an additional constraint parameter along with the stress intensity factor K for LEFM, or with the J-integral for EPFM to accurately describe the stress fields of a crack. The most commonly used constraint parameter is the elastic T-stress. Larsson and Carlsson (1973), Rice (1974), Bilby *et al*. (1986) suggested that the elastic T-stress can be used as the constraint parameter. They observed that the T-stress could affect the magnitude of the stress triaxality near the elastic-plastic crack tip field. A positive T-stress strengthens the crack tip triaxality and results in a high crack tip constraint while a negative T-stress reduces the crack tip triaxality and lowers the crack tip constraint. The late work by (Du and Hancock 1991, Betegon and Hancock 1992) further established the T-stress as an effective constraint parameter. Recently, the effect of T-stress is further studied for three-dimensional crack geometries (Meshii *et al*. 2010, Meshii and Tanaka 2010, Qian 2010, Gonzalez-Albuixech *et al*. 2011).

Failure assessment procedures which are commonly used in industrial applications are based on the conventional one-parameter fracture mechanics of K or J-integral. Therefore overly conservative assessment results would be obtained for low constraint conditions. It has been shown that by including the T-stress term into the conventional FAD, the low constraint effect can be accounted for which results in the increase of maximum load carrying capacity of the cracked structures (Ainsworth and O'Dowd 1995).

Hollow cylinder with an internal circumferential crack (Fig. 1) is a commonly used model in engineering structures such as those involved in pressure vessels and pipeline industries. For remote tensile loading, the cracked cylinder is under low constraint conditions. The realistic fracture assessments of these cracked cylinders using two-parameter, constraint-based fracture mechanics are of significant practical importance for the design and maintain of cylinders and pipelines. For this crack geometry, stress intensity factor solutions have been calculated extensively covering a wide range of radius ratio and crack depths, as summarized by Anderson (1991). However, only limited T-stress solutions have been obtained in the literature. Sherry *et al*. (1995) have provided the T-stress solutions for thin cylinders with circumferential cracks with radius ratio ranging from $r_i/r_o = 0.85$ to 0.95. Although J-integral analyses were also studied in the literature (Kumar *et al*. 1981), fully plastic J-integral solutions had been produced only for the circumferentially cracked thin cylinders ($r_i/r_o \geq 0.83$). Anderson (1991) summarized fully plastic J-integral results for cylinders with $r_i/r_o = 0.83$, 0.9, and 0.95. Further studies are required to calculate the fracture parameters such as T-stress and J-integral for a wider range of cylinder radius ratios and based on which the constraint-based assessment can be conducted.

In this paper, the constraint-based fracture mechanics analyses of hollow cylinders with internal circumferential crack under uniform tensile loading are conducted. Complete linear elastic and elastic-plastic finite element analyses of the cracked cylinder are carried out to determine the fracture parameters such as T-stresses and J-integral. The geometry of the hollow cylinder is shown in Fig. 1. The cylinder radius ratio that will be studied are $r_i/r_o = 0.2$ to 0.8, covering the wide range of thick to thin cylindrical geometries. For each cylinder radius ratio, cracks with depth ratio of $a/t = 0.2$ to 0.8 will be examined, covering both shallow to deep cracks. The fracture parameters will then be applied to construct both conventional and constraint-based failure assessment diagrams to determine the maximum load carrying capacities of the cracked cylinders.
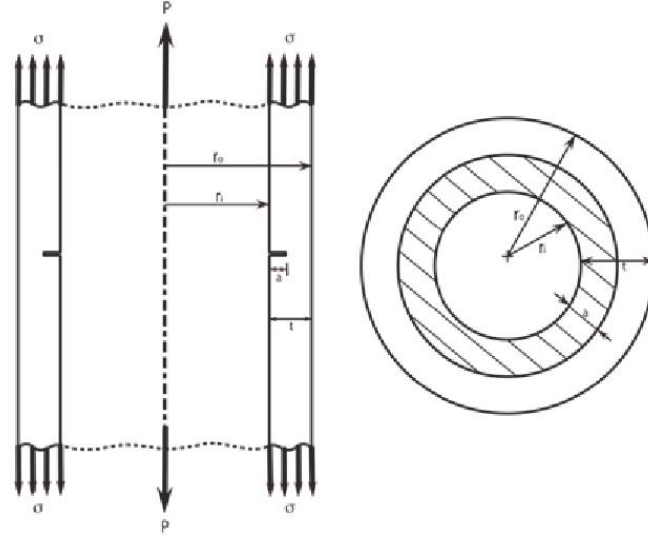
Fig. 1 Internal circumferential crack in cylinder

2. Solutions for fracture mechanics parameters

In this section, the solutions of elastic *T*-stresses and fully plastic *J*-integrals are determined for cracked hollow cylinders with r_i/r_o = 0.2, 0.4, 0.6 and 0.8 and a/t = 0.2, 0.4, 0.6 and 0.8.

2.1 Determination of the elastic T-stresses

In an isotropic linear elastic body containing a crack subjected to symmetric (Mode I) loading, the Williams series expansion (1957) of three-dimensional (3D) stress components near the crack tip can be written as

$$
\begin{bmatrix} \sigma_{11} & \sigma_{12} & \sigma_{13} \\ \sigma_{21} & \sigma_{22} & \sigma_{23} \\ \sigma_{31} & \sigma_{32} & \sigma_{33} \end{bmatrix} = \frac{K_I}{\sqrt{2\pi r}} \begin{bmatrix} f_{11}(\theta) & f_{12}(\theta) & 0 \\ f_{21}(\theta) & f_{22}(\theta) & 0 \\ 0 & 0 & f_{33}(\theta) \end{bmatrix} + \begin{bmatrix} T_{11} & 0 & 0 \\ 0 & 0 & 0 \\ 0 & 0 & T_{33} \end{bmatrix}
\tag{1}
$$

where σ_{ij} is the stress tensor, K_I is the stress intensity factor of mode I loading, r and θ are radial and polar coordinates centered at the crack tip, and f_{ij} is a dimensionless function of θ. The second order terms T_{11} and T_{33} in Eq. (1) are defined as *T*-stresses, they are the only non-zero and non-singular terms in the series expansion. Conventionally, T_{11} has been simply referred as *T*-stress while T_{33} is also called *S*-stress (Rice 1974). Physically T_{11} and T_{33} represent the stresses in the crack surface plane normal to and tangential to the crack front, respectively.

In a two-dimensional (2D) crack configuration, T_{33} is related to T_{11} by $T_{33} = \nu T_{11}$ under plane strain conditions, where ν is the Poisson's ratio. For 3D crack problems such as the case of circumferential cracks, T_{33} and T_{11} are independent, and both T_{11} and T_{33} are therefore generally required to characterize the crack tip stress fields (Meshii *et al.* 2010, Meshii and Tanaka 2010 and Gonzalez-Albuixech *et al.* 2011).
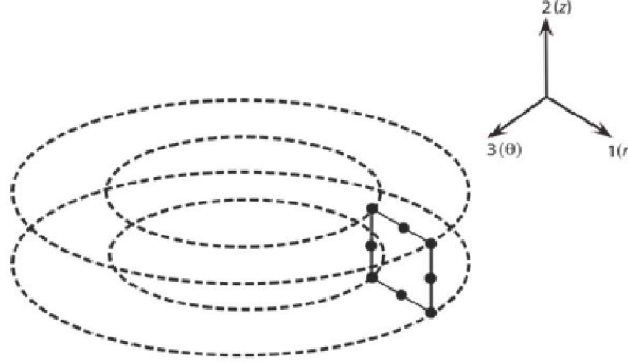
Fig. 2 Axisymmetric element used in the FEA

The elastic *T*-stress can be calculated by several methods such as the finite element method and the weight function method, see Lewis and Wang (2008), Wang (2002), for example. Determination of the elastic *T*-stress by finite element method using an interaction integral will be used here. Nakamura and Parks (1992) developed efficient method of extracting the *T*-stresses for three-dimensional fracture problems by introducing an interaction integral. The interaction integral is defined in the content of finite element analysis as

$$I(s) = \frac{1}{A_c} \int_{V_{(s)}} \left\{ \left(\sigma_{ij} \frac{\partial u_i^L}{\partial x_k} + \sigma_{ij}^L \frac{\partial u_i}{\partial x_k} \right) \frac{\partial q_k}{\partial x_j} - \sigma_{ij}^L \varepsilon_{ij} \frac{\partial q_k}{\partial x_k} \right\} dV \qquad (2)$$

where $V_{(s)}$ is a domain which encloses the crack front segment, $q_k(s)$ defines the virtual extension of the crack front segment and A_c is the increase in crack area generated by the virtual crack advance; $\sigma_{ij}, \varepsilon_{ij}$ and u_i are the stress, strain and displacement components of the 3D crack problem under consideration; $\sigma_{ij}^L, \varepsilon_{ij}^L$ and u_i^L are the corresponding components in the line-load auxiliary solution.

The crack tip T_{11}-stress is related to the interaction integral, $I(s)$, by the following Nakamura and Parks (1992)

$$T_{11}(s) = \frac{E}{1-v^2} \left\{ \frac{I(s)}{f} + v\varepsilon_{33}(s) \right\} \qquad (3a)$$

where $\varepsilon_{33}(s)$ is the extensional strain at point *s* in the direction tangential to the crack front. Once T_{11} is obtained, T_{33} can be obtained by the relationship with T_{11} and $\varepsilon_{33}(s)$, expressed as

$$T_{33}(s) = E\varepsilon_{33}(s) + vT_{11}(s) \qquad (3b)$$

Further details of this method can be found in Nakamura and Parks (1992), Qu and Wang (2006).

For the present internal circumferential cracks, both T_{11} and T_{33} will be calculated. In the current finite element analyses, *T*-stresses: T_{11} and T_{33}, are calculated from Eqs. (3a) and (3b) using the domain integral *I*(s) of Eq. (2). Eight-noded axisymmetric elements (see Fig. 2) are used in the finite element analyses using ABAQUS (ABAQUS 2008). The axisymmertic formulations of

Table 1 Normalized T_{11} and T_{33} stresses

Normalized T_{11}-stress, V_{11}					
a/t	$r_i/r_o = 0.9$	$r_i/r_o = 0.8$	$r_i/r_o = 0.6$	$r_i/r_o = 0.4$	$r_i/r_o = 0.2$
0.2	-0.56	-0.57	-0.57	-0.60	-0.69
0.4	-0.63	-0.65	-0.69	-0.74	-0.84
0.6	-0.87	-0.92	-0.98	-1.01	-1.04
0.8	-1.90	-1.91	-1.94	-1.84	-1.69
Normalized T_{33}-stress, V_{33}					
a/t	$r_i/r_o = 0.9$	$r_i/r_o = 0.8$	$r_i/r_o = 0.6$	$r_i/r_o = 0.4$	$r_i/r_o = 0.2$
0.2	-0.54	-0.58	-0.65	-0.73	-0.81
0.4	-0.72	-0.79	-0.88	-0.92	-0.92
0.6	-1.08	-1.16	-1.20	-1.15	-1.09
0.8	-1.82	-1.87	-1.83	-1.71	-1.54

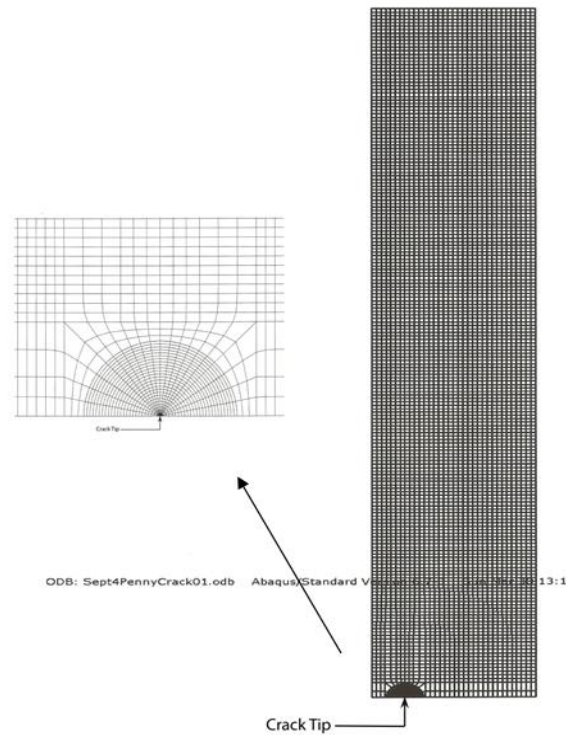ODB: Sept4PennyCrack01.odb   Abaqus/Standard V   13:1

Crack Tip

Fig. 3 Typical finite element model of cracked cylinder

Eqs. (2) to (3) are implemented in ABAQUS (ABAQUS 2008). To verify the finite element procedure of determining the *T*-stress, calculations using axisymmetric elements were performed for the geometry of a solid cylinder containing a penny-shaped crack under remote tension. Analytical solution of the *T*-stress for penny shaped crack was taken from Wang (2004) for comparison. The difference between the *T*-stress results had a maximum difference of 0.1%.

The *T*-stress analyses were then performed for crack lengths of a/t = 0.2, 0.4, 0.6 and 0.8 and cylinder thickness ratios of r_i/r_o = 0.2, 0.4, 0.6, 0.8 and 0.9. Fig. 3 shows a typical FE mesh used. To model the long cylindrical geometry, the length of the cylinder modeled is taken three-times longer the r_o. For each of crack geometry, the stress intensity factor was calculated first, and compared with the established stress intensity factor solutions (Anderson 1991). Excellent agreements were achieved for all the crack configurations analyzed, with maximum difference being within 2%. This serves as additional verification of the finite element models.

The interaction integral method was used to determine the *T*-stresses. Very good contour independence was obtained in these calculations (excluding the first contour). Seven contours were taken around the tip of the crack and the outer three contours were averaged and used as the *T*-stress value. The normalized *T*-stresses are given as

$$V_{11} = \frac{T_{11}}{\sigma} \tag{4a}$$

and

$$V_{33} = \frac{T_{33}}{\sigma} \tag{4b}$$

where V_{11} and V_{33} are the normalised *T*-stresses and σ is the nominal tensile stress. The *T*-stress results are tabulated in Table 1. Figs. 4 and 5 plot the results of the calculated *T*-stresses.

From the results shown in Figs. 4 and 5, it can be observed that the *T*-stresses (both T_{11} and T_{33}) calculated were negative. The negative *T*-stress indicates crack geometry under low constrained conditions. The T_{11} and T_{33} have very quite similar trends, for all cylinder radius ratios, as the crack depth (a/t) increases, the *T*-stresses decrease further down. Generally, for shallow cracks (small a/t ratios), the magnitude of *T*-tress is larger for thicker cylinders. This trend is reversed for deep cracks (large a/t values), that is, the magnitude of *T*-stress is smaller for thicker cylinders. This observation holds for both T_{11} and T_{33}.
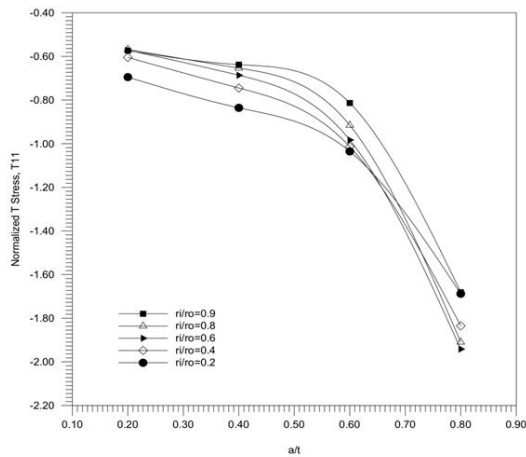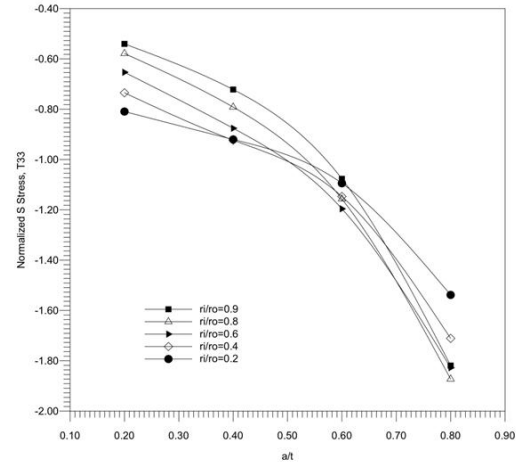

Fig. 4 Normalized T_{11} solutions   Fig. 5 Normalized T_{33} solutions

2.2 Determination of the fully plastic J-integral

Next, elastic-plastic finite element analyses were conducted to calculate the fully plastic *J*-integrals for internal circumferential cracks (Fig. 1). The analyses were performed using ABAQUS, with 8-noded axisymmetric elements. Similar mesh designs as shown in Fig. 3 were used in the calculations.

The material model used in the present calculations is deformation plasticity theory, Ramberg-Osgood mode as provided in ABAQUS

$$\frac{\varepsilon}{\varepsilon_0} = \frac{\sigma}{\sigma_0} + \alpha \left(\frac{\sigma}{\sigma_0} \right)^n \tag{5}$$

where α is a dimensionless constant, ε_0 is the yield strain, σ_0 is the yield stress, and *n* is the material-hardening coefficient. For all the analyses, $\alpha = 1$, $E = 207\text{GPa}$, $\sigma_0 = 200\text{MPa}$, and $\nu = 0.3$ were used. Three different *n* values, $n = 3$, 5 and 10, are considered to investigate both high and low strain hardening behaviours. Note the resulting fully plastic *J*-integral solutions, once normalized will be independent of the absolute material constant values of α, *E* and σ_0. They depend only on the geometry and hardening exponent. The finite element analyses use conventional small-strain theory.

The *J*-integral values were obtained using the domain-integral method provided in ABAQUS (2008). The *J*-integral obtained from the finite element analysis is the total integral consisting of two portions

$$J = J_e + J_p \tag{6}$$

where J_p is the plastic portion; while J_e is the elastic portion of the *J*-integral, and related to the stress intensity factor as follows

$$J_e = \frac{K^2}{E'} \tag{7}$$

where *E'* is the generalised Young's modulus: $E' = E$ for plane stress conditions, and $E' = E/(1-\nu^2)$ for plane strain conditions. Therefore, the fully plastic *J*-integral solutions, J_p, need to be extracted using the EPRI (Electric Power Research Institute) scheme.

As the magnitude of remote load σ increases, in the total *J*-integral results, the elastic portion of Eq. (6) becomes smaller and smaller. Once the fully plastic load level is achieved, the fully plastic J_p will then have the following proper $(n + 1)$ power dependence on the applied load, which can be written as

$$J_p = h_1 \alpha \sigma_0 \varepsilon_0 c \left(\frac{P}{P_0} \right)^{n+1} \tag{8}$$

where h_1 is the fully plastic factor, α, σ_0, ε_0 and *n* are the Ramberg-Osgood constants, *c* is the ligament ($= t - a$), and P_0 is the limit load for a hollow cylinder with internal circumferential crack given by Kumar (1981), Anderson (1991)

$$P_0 = \frac{2}{\sqrt{3}} \pi \left[r_o^2 - (r_i^2 + a)^2 \right] \sigma_0 \tag{9}$$

Table 2 Results of normalized fully plastic factor h_1

$r_i/r_o = 0.2$				
(n)	*a/t* = 0.2	*a/t* = 0.4	*a/t* = 0.6	*a/t* = 0.8
3	0.55	0.43	0.31	0.22
5	0.73	0.51	0.31	0.20
10	1.31	0.67	0.32	0.19
$r_i/r_o = 0.4$				
(n)	*a/t* = 0.2	*a/t* = 0.4	*a/t* = 0.6	*a/t* = 0.8
3	0.85	0.64	0.45	0.29
5	1.08	0.70	0.41	0.25
10	1.71	0.81	0.37	0.23
$r_i/r_o = 0.6$				
(n)	*a/t* = 0.2	*a/t* = 0.4	*a/t* = 0.6	*a/t* = 0.8
3	1.38	1.09	0.73	0.44
5	1.69	1.12	0.61	0.35
10	2.40	1.07	0.40	0.31
$r_i/r_o = 0.8$				
(n)	*a/t* = 0.2	*a/t* = 0.4	*a/t* = 0.6	*a/t* = 0.8
3	3.05	2.72	1.80	0.94
5	3.71	2.66	1.34	0.70
10	4.82	2.15	0.73	0.57

The fully plastic factor h_1 in Eq. (8) only depends on the strain hardening exponent n and the crack geometry. In the present analysis, the finite element program uses the standard technique of increment and iteration, which gradually increases the load magnitude until the fully plastic level is reached. After extensive verifications, a criterion has been set up in the present analysis to determine the achievement of fully plastic condition for the extraction of J_p. That is, if the J_p obtained from the analysis makes up more than 95% of the total J integral calculated (see Eq. (6)), the corresponding J_p is considered to be the fully plastic J-integral, based on which the h_1 factor is obtained from Eq. (8). Similar criterion was used to determined the J_p in surface cracks (Wang 2006).

Verifications were performed first to determine the validity of the present fully plastic J-integral calculation procedures. A penny-shaped crack in an infinite body under remote tension was analyzed first. The fully plastic h_1 factors were calculated for $n = 3$, 5 and 10. The results are in excellent agreement with results from He and Hutchinson (1981), with a maximum difference of 3.97%. Then the circumferential crack in a thin cylinder of $r_i/r_o = 0.83$ was analyzed for $a/t = 0.5$ and $n = 3$, 5 and 10. There was a maximum difference of 7.63 % between the calculated h_1 factor and the h_1 factors from Kumar *et al.* (1981) for the same crack configuration.

Elastic-plastic FE analyses were conducted to calculate the fully plastic J-integrals for the present crack configurations. The material property of the cylinder studied follows that of a Ramberg-Osgood power law hardening coefficient of $n = 3$, 5, and 10. The fully plastic geometry factor, h_1 is extracted from the fully plastic J-integral solutions based on Eq. (8). The solutions of h_1 factors for cylinders of $r_i/r_o = 0.2$, 0.4, 0.6 and 0.8; and $a/t = 0.2$, 0.4, 0.6 and 0.8 was determined. The h_1 factors are summarized in Table 2, and the results are plotted in Figs. 6-9.
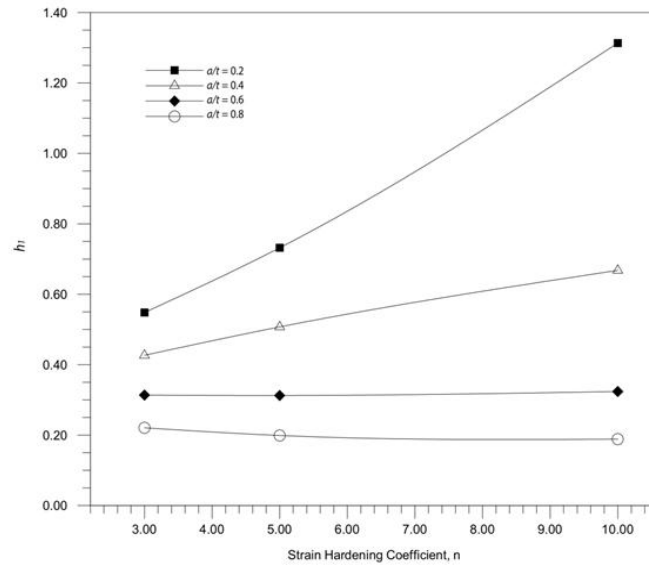
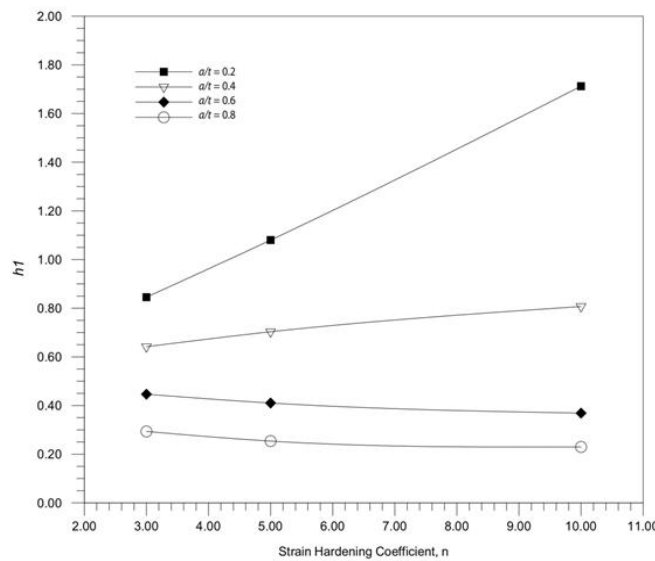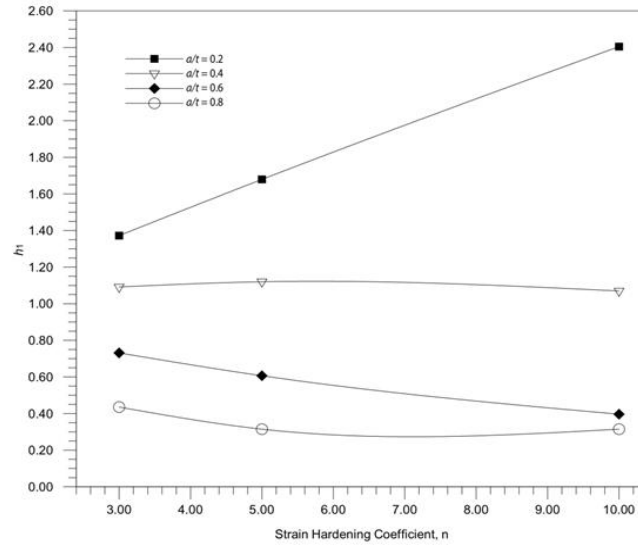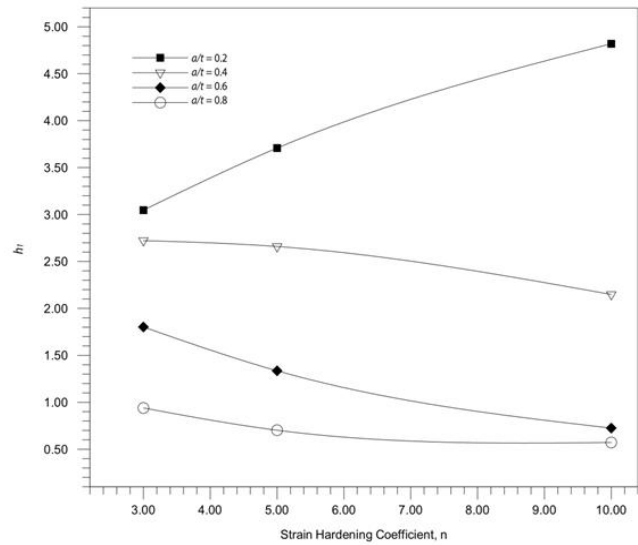Fig. 6 Fully plastic factor h_1 for cracked cylinders $r_i/r_o = 0.2$

Fig. 7 Fully plastic factor h_1 for cracked cylinders $r_i/r_o = 0.4$

It can be observed the for same strain-hardness exponent, h_1 factors decreases with crack depths for both thick and thin cylinders. Similar trends were observed for both thick cylinders ($r_i/r_o = 0.2$, 0.4) and thinner cylinders ($r_i/r_o = 0.6$, 0.8). Generally, the magnitude of h_1 is smaller in thicker cylinders comparing to thinner cylinders. From Figs. 6-9, it is be seen that generally h_1 factor increases with material hardening exponent n for shallow cracks ($a/t = 0.2$), and it decreases with n for deep cracks ($a/t = 0.6$ and 0.8).

Fig. 8 Fully plastic factor h_1 for cracked cylinders $r_i/r_o = 0.6$

Fig. 9 Fully plastic factor h_1 for cracked cylinders $r_i/r_o = 0.8$

3. Failure assessments of cracked cylinders

Based on the LEFM and EPFM fracture mechanics parameters obtained in last section, failure assessments can be conducted. The most commonly used failure assessment method is the failure assessment diagram method (R6 1997, Ainsworth *et al*. 2000, BS7910 1999). In this section, the constraint-based failure assessment diagram procedure is outlined first; then they were used to conduct failure assessments for cracked cylinders.

3.1 Constraint-based failure assessment diagrams

Consideration of the constraint effects in the failure assessment diagram approach was first introduced into the R6 procedure (R6 1997) and then included in SINTAP procedures (Ainsworth *et al*. 2000). The procedure that follows the R6 recommendations is outlined here, starting with the conventional method.

The conventional failure assessment diagram methods embedded in R6 (1997) and BS7910 (British Standard 1999) are essentially single parameter procedures in that fracture is assumed to be governed by a single value of toughness or crack opening displacement. The assessment of the potential of failure is determined by the two dimensionless calculated parameters, (K_r, L_r), determined from

$$K_r = \frac{K_I}{K_{IC}} \tag{10}$$

and

$$L_r = \frac{\sigma}{\sigma_L} \tag{11}$$

Here K_r is the stress intensity ratio with K_I being the stress intensity factor for the cracked component and K_{IC} the toughness of the material. The parameter L_r is the stress ratio, which is the ratio of the applied stress to the limit stress solution of the cracked component calculated based on the yield stress. Failure is avoided if this point (K_r, L_r) lies within a failure assessment diagram, represented by a curve, $K_r = f(L_r)$ and at the same time L_r is less than a cut-off value $L_r^{\max}$.

Based on two parameter fracture mechanics, R6 (1997) (Appendix 14) recognizes that a fracture resistance K_{mat}^C relevant to conditions of low constraint, may exceed the conventional fracture resistance K_{IC} measured under conditions of high constraint. To include this effect, it was suggested that the failure assessment diagram is modified to

$$K_r = f(L_r)(\frac{K_{mat}^C}{K_{IC}}) \tag{12}$$

Following detailed theoretical and experimental analysis (Ainsworth and O'Dowd 1995, Ainsworth *et al.* 2000), this increase in fracture toughness can be represented by the following relationship

$$K_{mat}^C = K_{IC}\left[1 + \alpha(-\beta L_r)^m\right] \tag{13}$$

where α, and m are material dependent constants, which define the dependence of fracture toughness on constraint; and β is a normalized constraint parameter. Substituting (13) into (12), we have

$$K_r = f(L_r)\left[1 + \alpha(-\beta L_r)^m\right] \tag{14}$$

Eq. (14) is the constraint-based failure assessment diagram. Failure is avoided if assessment point (K_r, L_r) (calculated from Eqs. (10) and (11)) lies within Eq. (14) and L_r is less than a cut-off value $L_r^{\max}$.

The normalized constraint parameter β is defined from the elastic *T*-stress or the hydrostatic *Q*-stress

$$\beta = \frac{Q}{L_r} = \frac{T}{\sigma_Y L_r} \tag{15}$$

where σ_Y is the yield stress of the material. Here, the following estimation of hydrostatic *Q* stress in terms of *T*-stress is used (Ainsworth and O'Dowd 1995)

$$Q = \frac{T}{\sigma_Y} \tag{16}$$

To conduct constraint-based assessment for a cracked body, in addition to the knowledge of the failure assessment curve $K_r = f(L_r)$, the stress intensity factor and the limit load for cracked components, the *T*-stress or the *Q* stress is required. Note that the material dependent constants α and *m*, used in Eq. (13) can be found for a wide range of materials in (Sherry *et al.* 2005). It is also important to note that Eq. (13) only applies for crack assessment under low constraint conditions (i.e., for $\beta < 0$). For high constraint conditions ($\beta \geq 0$), conventional FADs should be used.
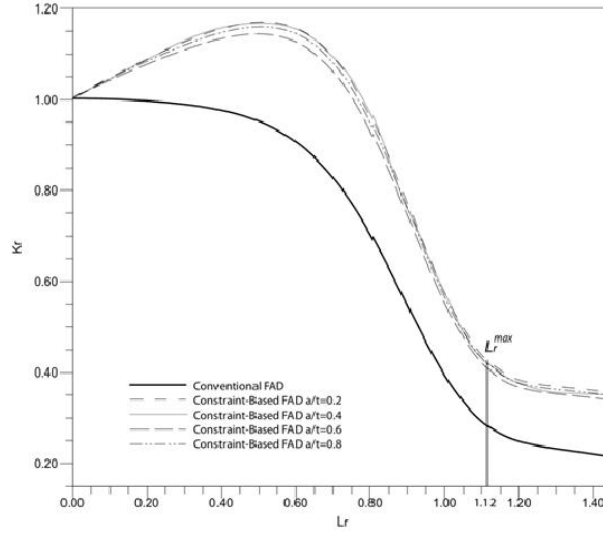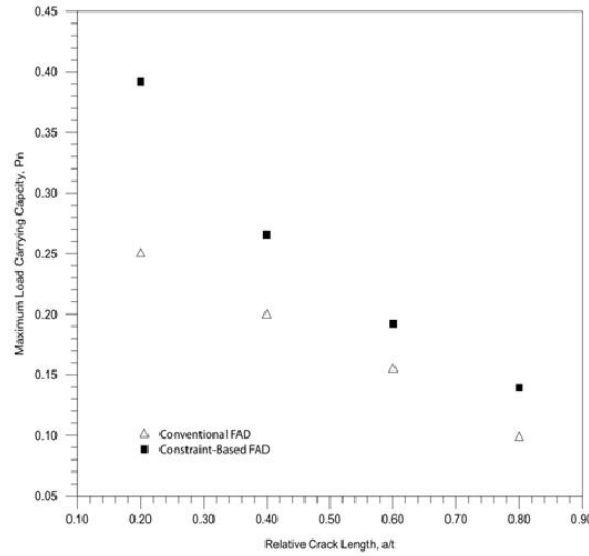
3.2 Failure assessment of cracked cylinders

Using the fracture parameters *T*-stresses and *J*-integrals, that were obtained in section 2 (Tables 1 and 2), together with the established stress intensity factor solutions as per Anderson (1991) and limit load solution, as per Eq. (9), the failure assessment diagrams for cracked cylinders can be constructed including the constraint effect. The failure assessment diagrams are generated for circumferentially cracked cylinders with thickness ratios of r_i/r_o = 0.2, 0.4, 0.6, and 0.8 and crack ratios of a/t = 0.2, 0.4, 0.6, and 0.8. The load applied to the cylinder is remote tensile loading. The material that was selected for the analysis is A533B, a typical pressure vessel low alloy steel. At operating temperature, the following material properties are used (ASME, 2001): tensile yield strength σ_y = 471 MPa, and ultimate strength σ_u = 591 MPa. The Young's modulus is 200GPa. The fracture toughness of the material is assumed to be K_{IC} is assumed to be 286 MPa $\sqrt{m}$ based on a conservative estimation. Constraint related material constants α, and *m*, which define the dependence of fracture toughness on constraint, are assumed to be 1.5 and 1 (Ainsworth and O'Dowd 1995), respectively. For each crack geometry, the maximum allowable remote tensile stress σ_{max} that can be applied without failure is obtained from the failure assessment diagram. The cracked cylinder is initially assessed using the conventional FAD procedure, and then reassessed using the constraint-based procedure.

In the present work, two levels of FAD approach were used. First, the lower bound FAD that is independent of geometry and material's stress-strain curve is used (Level 2A of BS7910 (1999))

$$K_r = f(L_r) = (1 - 0.14L_r^2)\left[0.3 + 0.7\exp(-0.65L_r^6)\right] \tag{17}$$

Since the load ratio is defined in terms of the yield strength, L_r can be greater than 1. The typical cut-off is 1.2 for C-Mn Steel and 1.8 for austentic stainless steel (BS7910 1999). In the current analysis, since the flow stress σ_f is known for the material used, which is equal to $0.5(\sigma_y + \sigma_u)$, the ratio of flow stress to the yield stress, σ_f/σ_y = 1.12, is used as the cut-off. Substituting (17) into (14), the resulting constraint based FAD is obtained

Fig. 10 Level 2A FADs (conventional and constraint-based) for cracked cylinder with $r_i/r_o = 0.2$

Fig. 11 Maximum stresses based on conventional and constraint-based FADs (Level 2A), $r_i/r_o = 0.2$

$$K_r = (1 - 0.14L_r^2)[0.3 + 0.7\exp(-0.65L_r^6)][1 + 1.5(-\beta L_r)] \tag{18}$$

Conventional (Eq. (17)) and constraint-based (Eq. (18)) FADs are constructed for cracked cylinders. Fig. 10 shows the conventional FAD together with the constraint-based FADs for $r_i/r_o = 0.2$ with varying a/t values from 0.2 to 0.8. Using these FADs, the maximum tensile stress σ_{max} are obtained for each crack configurations. The resulting maximum tensile stress σ_{max} is normalized as follows
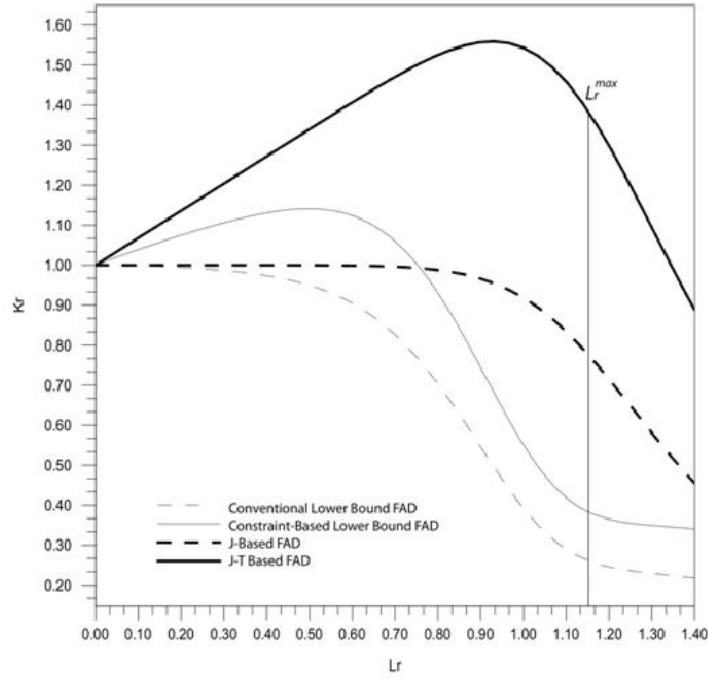
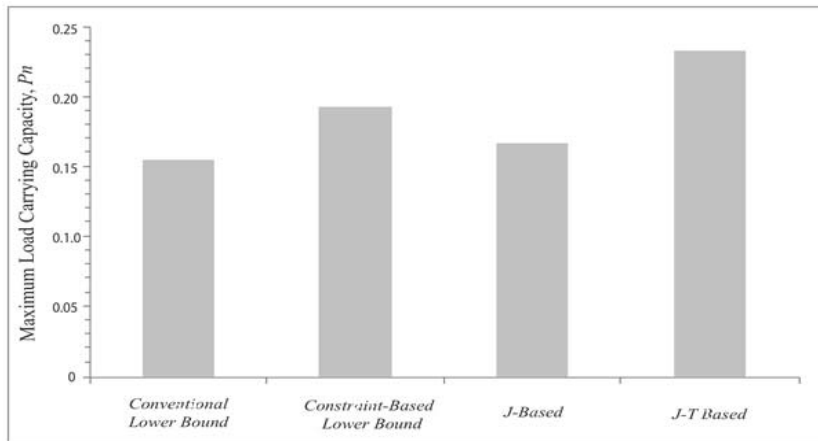Fig. 12 Level 2A and Level 3C FADs for cracked cylinder with r_i/r_o = 0.8, a/t = 0.6, n = 10

Fig. 13 Comparisons of P_n based on four FADs, for cylinder with r_i/r_o = 0.8, a/t = 0.6, n = 10

$$P_n = \frac{\sigma_{\max}}{\sigma_f} \tag{19}$$

where σ_f is the materials' flow stress. The maximum remote tension stress $\sigma_{\max}$ obtained using the conventional FAD was plotted in comparison with the constraint-based FAD in Fig. 11.

The comparison shows that for all crack depth ratio, the constraint-based FAD yielded a higher maximum load carrying capacity than the conventional FAD. Although not shown here, similar

observation were observed for thinner cylinders, r_i/r_o = 0.4, 0.6 and 0.8.

Next, the Level 3C analysis of BS7910 (1999) is conducted. It is a FAD depending on the geometry and material stress-strain curve. The failure assessment curve can be related to the solutions from the *J*-integral estimated based on the EPRI procedures (as discussed in section 2) and given as

$$K_r = f(L_r) = \sqrt{\frac{J_e}{J_e + J_p}} \qquad (20)$$

where J_e and J_p are values of *J*-integral obtained from elastic and elastic-plastic FEM analysis respectively. Substitute Eq. (20) into Eq. (14), the constraint-based FAD is obtained as

$$K_r = f(L_r) = \sqrt{\frac{J_e}{J_e + J_p}[1 + 1.5(-\beta L_r)]} \qquad (21)$$

Using Eq. (20) and Eq. (21), the FADs were generated for both the *J*-based method (Level 3C analysis) and *J-T* based methods (Constraint-based Level 3C analysis). The failure assessment diagrams are generated for circumferentially cracked cylinders with thickness ratios of r_i/r_o = 0.8, crack ratios of a/t = 0.6 and material hardening coefficient n = 10. Two sets of FADs are plotted, the first set is based on the lower bound (Level 2A) and constraint-based lower bound FAD (Constraint-based Level 2A) and the second set of curves are based on the *J*-based FAD (Level 3C) and *J-T* based FAD (Constraint-based Level 3C) for r_i/r_o = 0.8, a/t = 0.6. Both sets of FADs are shown in Fig. 12. Using the FADs in Fig. 12, the maximum stresses were obtained. Fig. 13 shows a summarized plot of the maximum load carrying capacity for the four different failure assessment diagrams. It is shown that the *J-T* based FAD (Constraint-based Level 3C FAD) resulted in the highest value of load carrying capacity. Note for the Level 3C analysis, only one crack/cylinder configurations and one material hardening exponent are shown here. Similar analyses can be conducted for other cylinder/crack geometries and material hardening exponents.

4. Conclusions

Linear elastic and elastic-plastic finite element analyses were conducted for circumferential cracked cylinders under remote tension loadings. The solutions of elastic *T*-stress and the fully plastic *J*-integrals for the circumferential cracks in hollow cylinders were determined. The analysis covered a wide range of cylinder radius ratios (r_i/r_o = 0.2 to 0.8) and crack depths (a/t = 0.2 to 0.8). It was shown that these cracked geometries are under low constraint conditions. The developed fracture mechanics parameters are complement to the available solutions in the literature.

Conventional and constraint-based failure assessment diagrams were developed using the developed solutions of fracture mechanics parameters together with the limit load solution. Two levels of conventional FADs (Level 2A and 3C of BS7910 (1999)) and the corresponding constraint-based FADs were constructed. The maximum load carrying capacities were determined using the FADs. Typical results for the cases of a thick cylinder (r_i/r_o = 0.2) and a thin cylinder (r_i/r_o = 0.8) are presented. It is demonstrated that the maximum load carrying capacities increase after accounting for the constraint effects comparing to results based on the conventional FADs.

The fracture mechanics parameter solutions of *T*-stress, *J*-integral obtained and the constraint-

based failure assessment procedures demonstrated in this paper enable a more realistic fracture assessment for these circumferentially cracked hollow cylinders.

Acknowledgements

References

ABAQUS, User's Manual (2008), Version 6.8, Habbitt, Karlsson& Sorensen Inc.

Ainsworth, R.A. and O'Dowd, N.P. (1995), "Constraint in the failure assessment diagram approach for fracture assessment", *ASME Journal of Pressure Vessel Technology*, **117**, 260-267.

Ainsworth, R.A., Sattari-Far, I., Sherry, A.H., Hooton, D.G. and Hadley, I. (2000), "Methods for including constraint effects within SINTAP procedures", *Engineering Fracture Mechanics*, **67**, 563-571.

Anderson, T.L. (1991), "Fracture mechanics: fundamentals and applications", *Boca Raton: CRC Press*, **91**, 283-298.

ASME, Boiler and Pressure Vessel Code, Section II, Materials, 2001 Edition.

Betegon, C. and Hancock, J.W. (1991), "Two-parameter characterization of elastic-plastic crack tip fields", *ASME Journal of Applied Mechanics*, **58**, 104-110.

Bilby, B.A., Cardew, G.E., Goldthorpe, M.R. and Howard, I.C. (1986), "A finite element investigation of the effect of specimen geometry on the fields of stress and strain at the tips of stationary cracks", *Size Effect in Fracture, London: Mechanical Engineering Publications Limited*, 37-46.

BS97910 (1999), "Guide on methods for assessing the acceptability of flawsin metallic structures", British Standards Institution.

Du, Z.Z. and Hancock, J.W. (1991), "The effect of non-singular stresses on crack tip constraint", *Journal of Mechanical Physics and Solids*, **39**, 555-567.

Gonzalez-Albuixech, V.F., Giner, E., Fernandez-Seaz, J. and Fernández-Canteli, A. (2011), "Influence of the T_{33}-stress on the 3D stress state around corner cracks in an elastic plate", *Engineering Fracture Mechanics,* **78**, 412-427.

He, M.Y. and Hutchinson, J.W. (1981), "The penny-shaped crack and the plane strain crack in an infinite body of power-law material", *ASME Journal of Applied Mechanics,* **48**, 830-840.

Kumar, V., German, M.D. and Shih, C.F. (1981), "An engineering approach for elastic-plastic fracture analysis", EPRI Report NP-1931, Electric Power Research Institute, Palo Alto, CA.

Larsson, S.G. and Carlsson, A.J. (1973), "Influence of non-singular stress terms and specimen geometry on small-scale yielding at crack-tips in elastic-plastic materials", *Journal of the Mechanics and Physics of Solids*, **21**, 447-473.

Lewis, T. and Wang, X. (2008), "The *T*-stress solutions for through-wall circumferential cracksin cylinders subjected to general loading conditions", *Engineering Fracture Mechanics*, **75**, 3206-3225.

Lidbury, D.P.G., Sherry, A.H., Bass, B.R. *et al.* (2006), "Validation of constraint-based methodology in structural integrity of ferritic steels for nuclear reaction pressure vessels", *Fatigue and Fracture of Engineering Materials and Structures*, **29**, 829-849.

Meshii, T. and Tanaka, T. (2010), "Experimental T_{33}-stress formulation of test specimen thickness effect on fracture toughness in the transition temperature region", *Engineering Fracture Mechanics,* **77**, 867-877.

Meshii, T., Tanaka, T. and Lu, K. (2010), "*T*-stress solutions for a semi-elliptical axial surface crack in a cylinder subjected to mode I non-uniform stress distributions", *Engineering Fracture Mechanics,* **77**, 2467-2478.

Nakamura, T. and Parks, D.M. (1992), "Determination of elastic *T*-stress along three dimensional crack fronts using an interaction integral", *International Journal of Solids and Structure*, **29**, 1597-1611.

Qian, X. (2010), "K_I-T estimations for embedded flaws in pipes - Part I: axially orientated cracks", *International Journal of Pressure Vessels and Piping*, **87**, 134-149.

Qu, J. and Wang, X. (2006), "Solutions of T-stress for quarter-elliptical corner cracks in finite thickness plates subject to tension and bending", *International Journal of Pressure Vessels and Piping*, **83**, 593-606.

R6 (1997), "Assessment of the integrity of structures containing defects, procedure R6, Revision 3", Nuclear Electric Ltd, Gloucester, U.K.

Rice, J.R. (1974), "Limitations to the small scale yielding approximation for crack tip plasticity", *Journal of the Mechanics and Physics of Solids*, **22**, 17-26.

Sherry, A.H., France, C.C. and Goldthorpe, M.R. (1995), "Compendium of *T*-stress solutions for two and three dimensional cracked geometries", *Fatigue Fracture Engineering Material Structure*, **18**, 141-155.

Sherry, A.H., Wilkes. M.A., Beardsmore, D.W. and Lidbury, D.P.G. (2005), "Material constraint parameters for the assessment of shallow defects in structural components—Part I: Parameter solutions", *Engineering Fracture Mechanics,* **72**, 2373-2395.

Wang, X. (2002), "Elastic *T*-stress for cracks in test specimens subjectedto non-uniform stress distributions", *Engineering Fracture Mechanics*, **69**, 1339-1352.

Wang, X. (2004), "Elastic *T*-stress solutions for penny-shaped cracks under tension and bending", *Engineering Fracture Mechanics*, **71**, 2283-2298.

Wang, X. (2006), "Fully plastic *J*-integral solutions for surface cracked plates under biaxial loading", *Engineering Fracture Mechanics,* **73**, 1581-1595.

Williams, M.L. (1957), "On the stress distribution at the base of a stationary crack", *ASME Journal of Applied Mechanics*, **24**, 111-114.